Spatiotemporal Patterns on a Ring Array of Electrodes

Z. Fei, B. J. Green, and J. L. Hudson*

Department of Chemical Engineering, Thornton Hall, University of Virginia, Charlottesville, Virginia 22903-2442

Received: July 31, 1998; In Final Form: January 4, 1999

Experiments have been carried out with a ring array of iron electrodes in sulfuric acid under conditions in which high-frequency periodic and chaotic oscillations occur. All the electrodes were held at the same constant potential. The currents of the electrodes were measured independently, and therefore, the spatiotemporal patterns in current density which occurred were directly determined. Depending on the conditions of the experiments, primarily applied potential, and also solution concentration, a variety of periodic and chaotic oscillatory spatiotemporal patterns arose. The simplest case, a uniform periodic oscillation, does occur, but it is not the most common state. With a change of parameter, higher modes become important. One set of changes among pattern types with variation of potential, including an apparent period doubling, is investigated in detail. Other types of behavior including antiphase oscillations and chaotic patterns were also observed.

Introduction

Spatiotemporal patterns occur in a variety of electrochemical systems including electrodissolution, electrodeposition, and electrocatalytic reactions. The local reaction rate or current, the potential outside the double layer, and species concentrations can then be functions of the position on the electrode surface. Although many studies have been made of time-varying phenomena, such as oscillations in electrochemical systems,[1] there has been somewhat less done in cases in which variations in both time and space occur. Nevertheless, the existence of spatial patterns in electrochemical systems has been known for some time. For example, in 1907 Heathcote published a study on the propagation of an active area on an iron wire in nitric acid,[2] and about 20 years later Lillie described related results.[3]

Spatial patterns can occur in the bistable, oscillatory, or excitable regions. Bistability has been observed during metal dissolution, near the active−passive transition, and in electrocatalytic systems; in both cases, a simple model in which potential serves as the dependent variable can reproduce the qualitative features of the system. In the bistable region, transitions from one state to another can be associated with accelerating reaction fronts.[4,5] Oscillatory behavior is common in electrochemistry and is typically modeled using the potential in the electrolyte and species concentration as the two variables. The autonomous oscillations in current and/or potential that occur during the electrodissolution of metals[6−9] and during electrocatalytic reaction[10,11] are often accompanied by spatial patterns that vary with time.[12−18] Rotating waves have also been observed[19] in the oscillatory region. Under excitable conditions, pulses can propagate along the electrode surface in a monotonic or modulated fashion.[15]

In some recent papers we have discussed spatiotemporal patterns observed during the dissolution of iron in sulfuric acid using arrays of electrodes.[20−22] The arrays consist of a number of small disks that are made from the ends of wires embedded in an insulator. The current in each of the electrodes is measured independently, and the patterns can be obtained from the current signals. An array of electrodes behaves approximately like a larger, single electrode of the same total area.[20] This similarity exists because much of the coupling in the electrochemical system is through the electrolyte and long-range effects are important. In the parameter region in which fast oscillations occur, transition from period to chaotic to higher dimensional chaos was seen as the number of electrodes increased.[22]

The long-range coupling through the electric field is an important characteristic of electrochemical systems, and it can have an important role in the type of patterns that occur.[23−27] It is a coupling that is not global since the coupling strength depends on the distance between sites but which is also not local since events at one location can affect events at distant locations directly. This coupling has been shown to cause the front acceleration that was mentioned above.[4,5,26]

Of some relevance to the present paper are studies of patterns on the ring geometry in electrochemical[17,19] and gas−solid catalytically reacting systems.[28−33] Patterns such as rotating pulses, back-and-forth swinging pulses, and alternating hot spot formation at two locations have been reported by Luss and coworkers in experimental studies of gas−solid reactions on catalytic rings;[28,31] rotating pulses have been seen in experiments on CO oxidation on a ring by Yamamoto et al.[32] Furthermore, Middya et al. showed through simulations that global coupling can lead to patterns not seen in reaction−diffusion systems;[29] they used a simple cubic-type rate expression to study the effects of global coupling on a ring and showed that although the rotating pulse is the predominant pattern, antiphase oscillations and crossing pulses can occur.[29]

Rotating waves can be created in oscillatory electrochemical systems by the simple placement of the reference electrode.[19] The imposed potential drop between the working and reference electrodes is controlled by the current flow between working and counter electrodes. Spatial variations of the potential in the body of the electrolyte occur; in the simplest case, the potential field is governed by the Laplace equation.[5,25] The position of the reference electrode influences the potential field along the working electrode outside the electrical double layer. Consider the case of a ring working electrode in which the reference electrode is placed on the center line and far from the working electrode and in which simple oscillations with no spatial

10.1021/jp983252j CCC: $18.00
Published on Web 03/04/1999

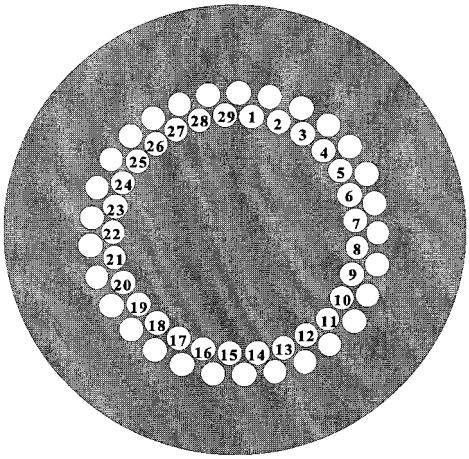

Figure 1. Configuration of the ring electrode.

dependence along the ring, i.e., in the angular direction, occur. (Similar arguments can be made for a disk electrode, but in this case there are radial variations.) As the reference electrode is brought closer to the plane of the electrode along the center line, the uniform oscillations can be changed to a rotating wave with an almost constant total current. The rotating wave is caused by negative long-range coupling through the electric field. A reaction or current flow at one point of the ring tends to inhibit reaction at a point displaced by 180°[27] In the experiments described in the present paper, the ratio of the distance between the reference and working electrodes to the size of the working electrode is 20 to 7 or approximately 3. At this large ratio no negative coupling and thus no rotating waves are expected; and none was seen. It is interesting that the rotating pulses occur in the gas−solid reaction systems with positive global coupling but have not been seen in electrochemical systems, except in the presence of the negative coupling.

In this work we report the results of experimental studies of patterns on a ring array of electrodes. The system is that of iron electrodes in sulfuric acid in an impinging jet. Under the conditions of the experiments, a single electrode would undergo fast (approximately 86 Hz with no added ferous sulfate) period-one oscillations. The working electrode consists of two concentric rings, each consisting of 29 electrodes; however, only the current on the inner ring was measured. Although a uniform oscillation is observed, it is not the predominant behavior; higher modes are more commonly important. Several spatiotemporal patterns not seen in previous experiments with electrochemical or other type of chemical reaction are observed. Transitions among pattern types, both periodic and chaotic, are seen as the applied potential is changed. The possible role of coupling in producing the observed patterns is discussed.

Experimental Section

The configuration of the electrode ring array is shown in Figure 1. The ring consists of 58 individual electrodes arranged in two concentric circles of 29 electrodes as shown. The experiments were done potentiostatically. The currents of the inner 29 electrodes were measured individually; in addition, the total current of all 58 electrodes was obtained. The electrodes are numbered from 1 to 29 starting at the top and going clockwise; sometimes the angle is used, in which case zero is electrode number one and the angle is again measured in the clockwise direction. Each electrode is made from pure iron wire (Aldrich Chemical Co., Inc., 99.99+%) of diameter 0.5 mm. The distance between the wires is less than 0.05 mm. The electrodes are embedded in epoxy, and reaction takes place only on the ends. The diameter of the ring of electrodes is approximately 7 mm, and that of the epoxy matrix is 33 mm. Before each experiment, the electrode surface was polished with 400 grit silicon carbide paper. The electrode array faces downward. An impinging jet, flowing upward, was used to control the mass transfer coefficient at the electrode surface; the jet was about 20 mm from the electrode, and the mean jet speed was 18 cm/s. The reference electrode, a standard $Hg/Hg_2SO_4/K_2SO_4$ electrode, was placed next to the jet, i.e., about 20 mm from the surface of the working electrode. The counter electrode is a platinum foil in the shape of a ring with diameter of 65 mm. The counter electrode was approximately in the plane of the working electrode; moving it to a position farther from the working electrode had a negligible effect on the results.

Experiments were carried out in 1 M H_2SO_4 solution; in some cases, ferrous sulfate was added to the solution to a concentration of 0.002 M. The volume was 300 mL.

A Pentium PC installed with a 32 channel data acquisition board (Keithley DAS-1800HC2) was used for data sampling. Both the total current and the currents of the individual electrodes can be measured simultaneously. The sampling frequency is 2500 Hz and up to 5000 Hz for some cases.

The electrochemical reaction was controlled by a potentiostat (EG&G Princeton Applied Research, model 273). Electrodes in the array link to working electrode jacks of the potentiostat through a ZRA box (zero resistance ammeters). The ZRA circuitry consists of an operational amplifier and associated feedback circuitry such that currents in the range of 10^{-9} to 10^{-2} A may be measured for each electrode in an array without altering the polarization potential of the electrodes.

The experiments were done potentiostatically. The potential was first fixed at −180 mV ($Hg/Hg_2SO_4/K_2SO_4$), and the potential was then ramped in the cathodic direction at a rate of 2.5 mV/s to the desired value and held there; after stationary conditions were reached and measurements made, the potential was ramped to the new desired value and measurements again made. In a few cases the ramping was also done at a rate of 1.0 mV/s and no discernible difference was noted. The potential was held at a fixed value every 10, sometimes 5, mV, i.e., the potential was ramped down from −180 to −190 mV, held and measurements made, ramped to −200 mV, etc.

Results

Sequence of Spatiotemporal Patterns: $[FeSO_4] = 0.002$ M. Sets of experiments were done by holding conditions such as jet speed and electrolyte concentration constant and by using the applied potential as a control parameter. The results from one such set of experiments, at four values of the applied potential, are shown in Figure 2; the concentration of $FeSO_4$ in these experiments was 0.002 M. For an applied potential of −150 mV (Figure 2a), a periodic time series (not shown) for the total current of all 58 electrodes was obtained. The currents of the 29 electrodes comprising the inner ring were also measured individually. (The individual currents of the outer ring were not measured.) We are thus considering a narrow, approximately one-dimensional ring, and we only measure angular variations of current; on a wider ring or a disk electrode, the current can also be a function of radial position.[16,17] The current is represented by shading, black being low current and white high. The snapshot shows the current at a single instant in time. The space/time plot is a representation of the current as a function of position (angle measured in a clockwise direction starting from the top of the array as sketched) and

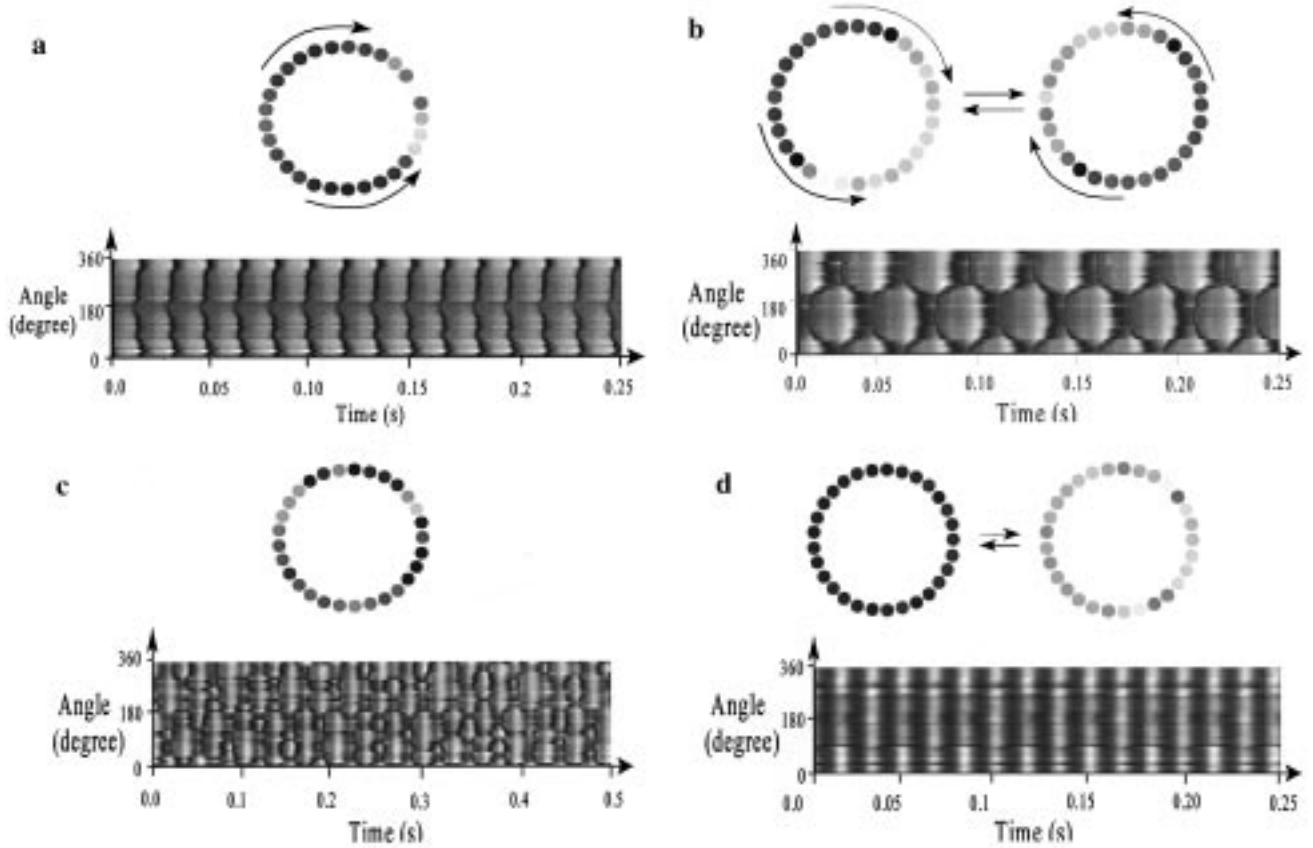

Figure 2. Snapshots and space/time current densities. Black represents low current and white high current. Jet speed = 18 cm/s, $[Fe^{2+}] = 0.002$ M. (a) Unidirectional wave, $E = -150$ mV (Hg/H_2SO_4). (b) Anti-phase oscillations, $E = -250$ mV (Hg/H_2SO_4). (c) Chaos, $E = -300$ mV (Hg/H_2SO_4) (d) Coherent oscillations, $E = -350$ mV (Hg/H_2SO_4).

time. The oscillation is period one; the pattern repeats itself every cycle of the time series. The current of each electrode oscillates periodically between a maximum and minimum value and thus is alternately shaded light and dark. The oscillations are far from harmonic; the dark (low current) portions of the cycle are relatively short compared to the much longer lighter (high current) portions.

The oscillations shown in Figure 2a are not uniform on the individual electrodes. The entire signal is made up of a mean (independent of time) component, an almost uniform component that varies periodically with time, and a higher mode. The oscillations on all of the individual electrodes are all periodic with the same period, but as can be seen from the space/time plot, they are not identical. Furthermore, the individual oscillators are not in phase. The length of time at which the electrodes are in the low-current state is much shorter that the times at which the current is high. Therefore, there are times in the cycle when the entire ring is in the high-current state. It is convenient in describing a cycle to begin at a time at which the electrodes are all at a high current so that all positions are shaded light. The current first begins to drop at a location of approximately 210°; the current at neighboring locations at both sides decreases with a phase lag. A wave thus propagates in both directions. The clockwise propagating branch travels to the opposite side of the array and ends at approximately 30°. During this traverse, the currents on the individual electrodes decrease as the wave front passes, all are briefly at a low current value, but then the currents sequentially increase as the waveback reaches the electrodes. In Figure 2a there appears to be a second location at approximately 100° that also has a phase that leads that of its neighbors. We have carried out several experiments at somewhat different conditions in which the resulting pattern is similar to that shown in Figure 2a. Another, shown in Figure 7a, will be discussed below. In some cases (as in Figure 2a), there appear to be two leading points separated by some finite angle. In other cases the separation angle is very small, and sometimes there appears to be only a single leading point. Note that all the dark stripes in the space−time plot are (aside from the small region between the two apparent leading points) convex from the prospective of increasing time. We have also converted these images into video pictures; the dominant pattern in the data of Figure 2a is a wave that propagates from the lower left to upper right of the array, and this direction is indicated in the snapshot. The waves from the perspective of a single location appear to be propagating in the same direction during all cycles.

Additional, quantitative information can be obtained on the characteristics of the experimental data by the use of the Karhunen−Loeve expansion, or proper orthogonal decomposition. A set of basis functions is determined empirically, and the spatiotemporal data are expanded on them. Both the eigenfunctions and the time-dependent coefficients are determined by the decomposition.[34] The method is useful in elucidating complex patterns and has been used successfully in analyzing data from reacting systems.[35−38] The signals, which are functions of both space and time, are expanded in an orthogonal set of eigenfunctions. The results of the decomposition for the data of Figures 2a are shown in Figure 3a.

The pattern of Figure 2a is a simple wave. Ninety-five percent of the energy is contained in the first two terms of the expansion. The first eigenfunction is approximately constant. Its coefficient is a periodic relaxation oscillation. A one-term expansion (over 70% of the energy) would be a uniform oscillation. The second eigenfunction is a function of position; its coefficient is a periodic signal that has a phase lag relative to the first

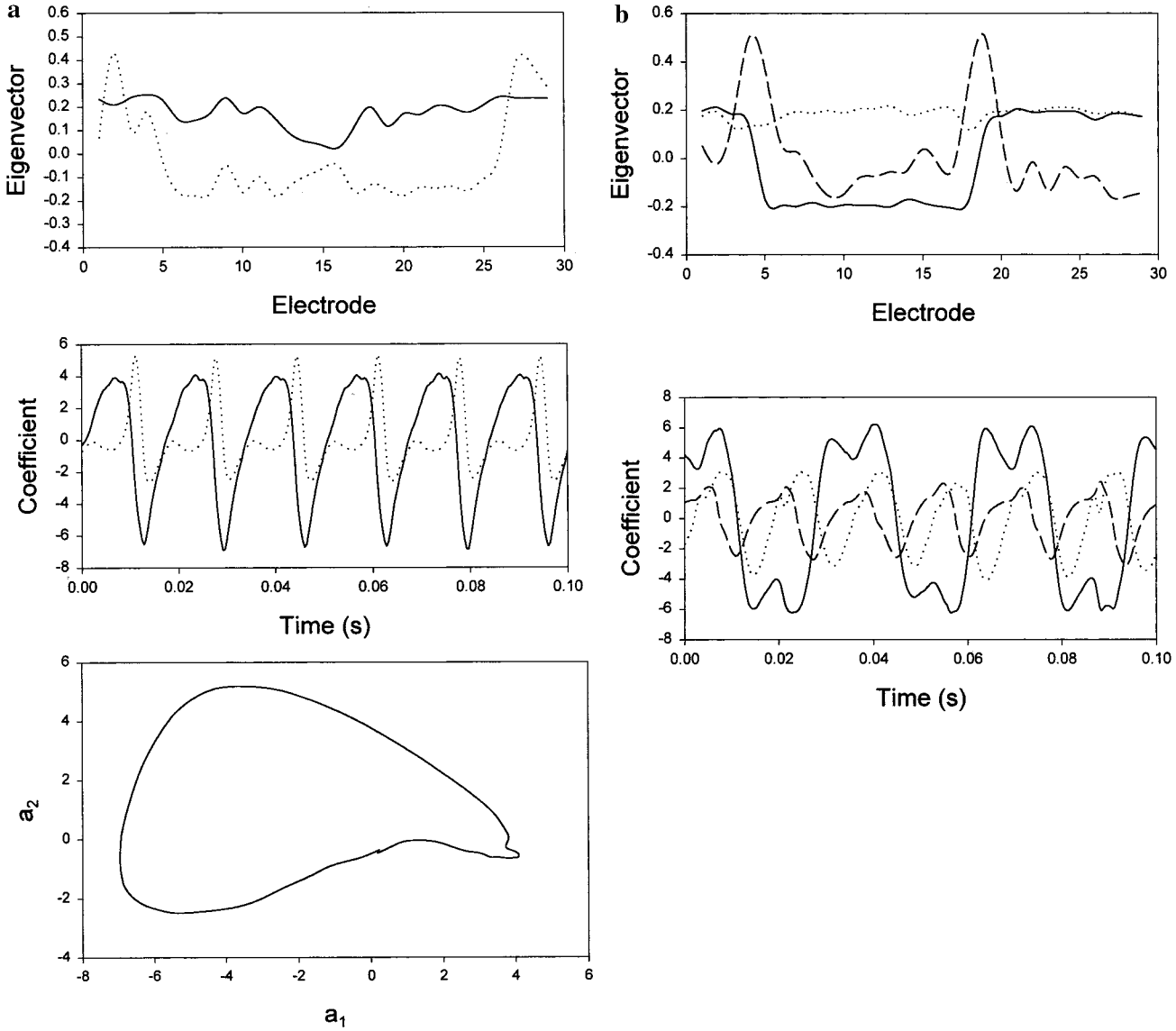

Figure 3. (a,b) Eigenvectors and coefficients from $K-L$ decomposition of the patterns in Figure 2a and 2b, respectively. Solid line, first term; dotted line, second term; dashed line, third term (when shown).

coefficient. The combination of these two terms can produce the essential features of the spatiotemporal pattern. We see then that the entire current pattern is made up of a mean (steady) value of 3.3 mA, a uniform nonharmonic oscillation of approximate amplitude 0.8 mA, and a spatially dependent component. The first two temporal coefficients a_1 and a_2 are shown again at the bottom of Figure 3a; the nature of the pattern can be seen by following one cycle. Start at the point at which a_1 is zero and where a_2 is very small. The first coefficient a_1 rises while a_2 remains close to zero. This is simply an almost uniform increase in current. Then a_1 decreases while a_2 decreases, which corresponds to the current decrease first at one location and then in succeeding positions across the ring.

In Figure 2b a snapshot and a space/time plot are shown for a somewhat lower potential, i.e., $E = -250$ mV, all other conditions the same. The time series of total current (not shown) is again periodic. The behavior of each individual electrode is, of course, also periodic. There is an important difference in the behavior between that of Figure 2b and that of Figure 2a. In Figure 2b the current first begins to drop alternately at two locations on the ring, at approximately 300° and 120°. Note in the space−time plot that the black curves are alternately convex and concave. Antiphase oscillations, superimposed on an additional uniform oscillation, occur. It can be seen in the space/time plot that the section of the ring from about 30° to 210° is usually in the opposite state as the remainder, from about 210° to 30°. The transition from the state in which one-half is high to the other being high occurs with a wave motion, but this wave is faster than that seen above in Figure 2a. The waves propagate alternatively from upper left (300°) to lower right (120°) and from lower right to upper left. The frequency of the complete cycle is 30 Hz. During a period of 0.033 s, the total current goes through two maxima.

The decomposition for the oscillations of Figure 2b is given in Figure 3b. In this case, three terms are required to capture about 95% of the energy. The first eigenfunction shows the structure associated with an antiphase oscillation, viz., one-half the array at one value and the other half at the same absolute value but opposite sign. The period of the oscillations is 0.033 s. Antiphase oscillations can be reconstructed using just two terms; such reconstructed antiphase oscillations, however, do not have the same behavior seen in Figure 2b, i.e., the regions of high and low current on the array simply switch back and forth. To produce the experimentally observed wave pattern, the third term must be included in the expansion. In this case, the second eigenfunction is approximately independent of spatial

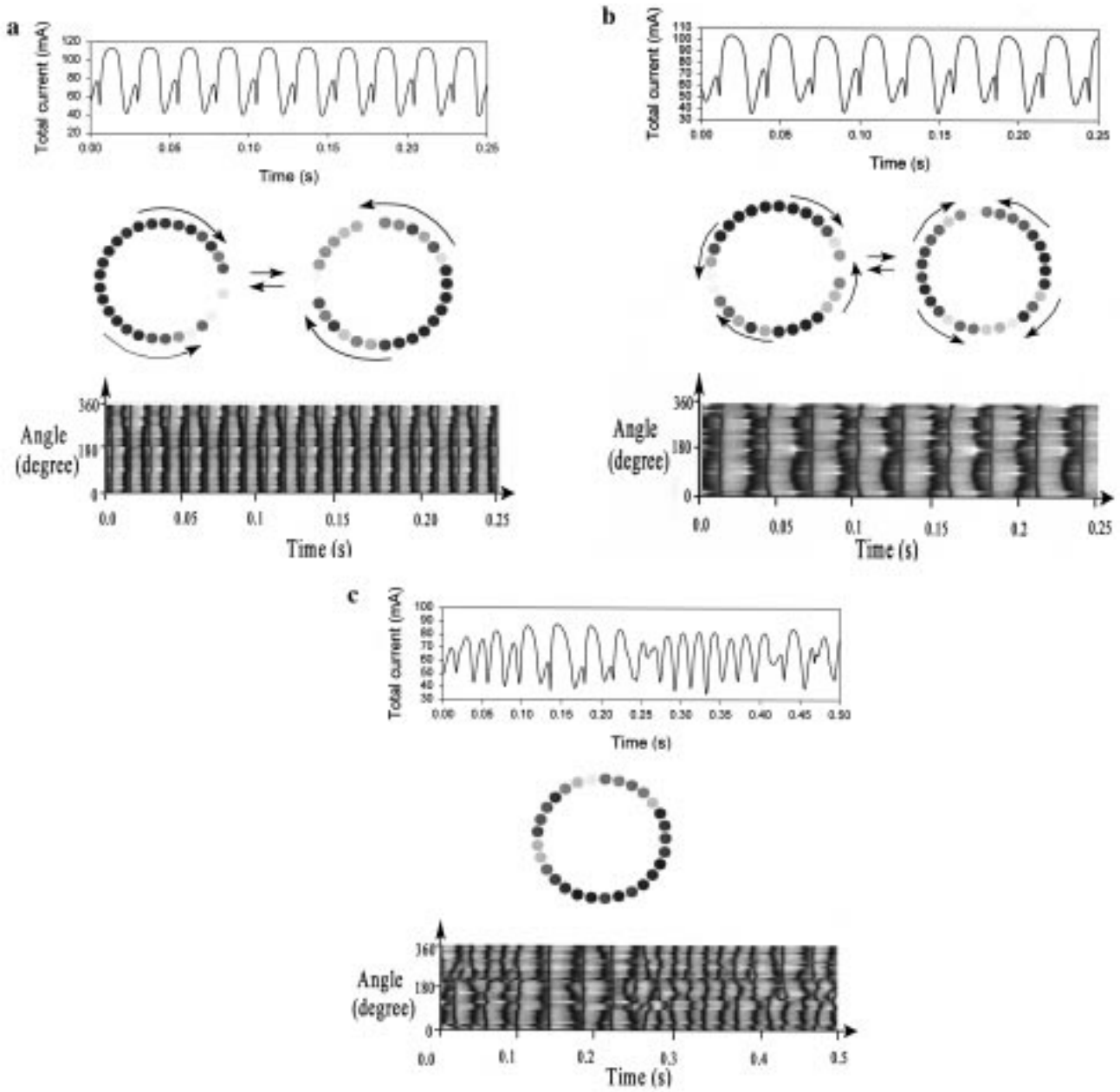

Figure 4. Time series of total current, snapshots, and space/time current densities. Black represents low current and white high current. Jet speed = 18 cm/s, $[Fe^{2+}] = 0.0$ M. (a) Bidirectional wave, $E = -225$ mV (Hg/H_2SO_4). (b) Cross-directional wave, $E = -250$ mV (Hg/H_2SO_4). (c) Chaos, $E = -300$ mV (Hg/H_2SO_4).

position and the second term in the expansion thus furnishes a component of uniform oscillation. The third term adds the wave propagation.

Decreasing the applied potential results in chaotic behavior, as seen in Figure 2c. There are a number of waves moving on the ring in no organized pattern. Nevertheless, remnants of the antiphase oscillations seen in Figure 2b remain. There are times in which one-half the ring is still almost in a high current state while the other is low and these behaviors switch, i.e., the high becomes low and the low high. The behavior appears to be chaotic, however, both in local and total current.

The chaotic behavior of Figure 2c was also decomposed. About 15 terms were necessary to represent the data. This was seen from the energy spectrum and also from the reconstruction; about 15 terms are necessary to produce video images that resemble those of the original data.

Further lowering of the potential brings the system back into periodic behavior, as seen in Figure 2d. This is the simplest state seen; the electrode array is almost uniform. The entire array simply oscillates uniformly with all individual electrodes oscillating in phase between states of high and low current.

Decomposition of the data of Figure 2d was also carried out but also is not shown. Only one term is necessary to capture 95% of the energy, and its eigenfunction is independent of position. Of course, if the oscillation were exactly uniform, one term with a flat eigenfunction would perfectly represent the dynamics. The second term (5%) has an eigenfunction that depends on position, and this term represents the deviation from uniform oscillations.

Second Sequence of Patterns: $[FeSO_4] = 0.0$ M. We now turn to a second set of experiments, the results of which are shown in Figure 4. These experiments are done without the added ferrous sulfate. Again the control parameter is the applied potential, which is held at a sequence of fixed values with other conditions held constant. The behavior at a potential $E = -225$ mV is shown in Figure 4a. Both the individual currents and the

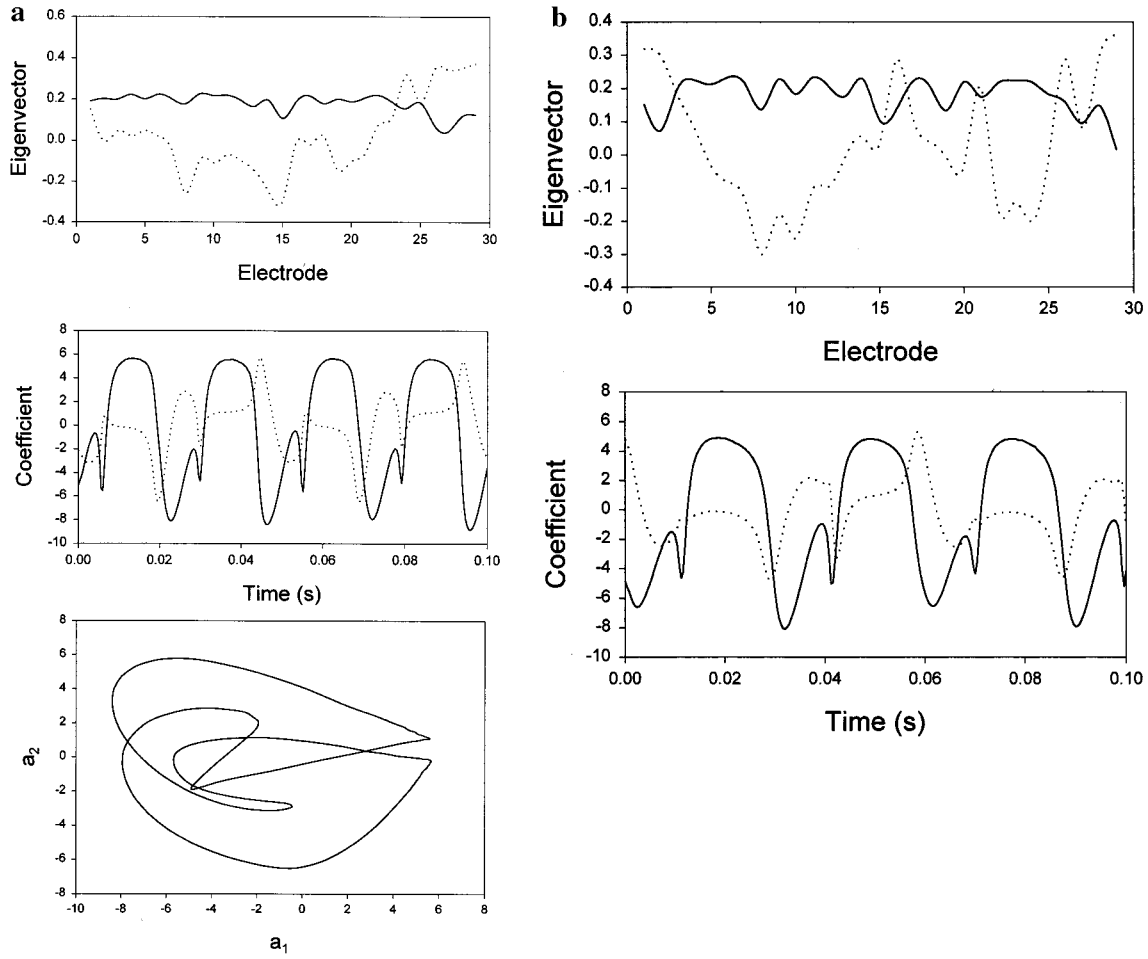

Figure 5. (a,b) Eigenvectors and coefficients from $K-L$ decomposition of the patterns in Figure 4a and 4b, respectively. Solid line, first term; dotted line, second term.

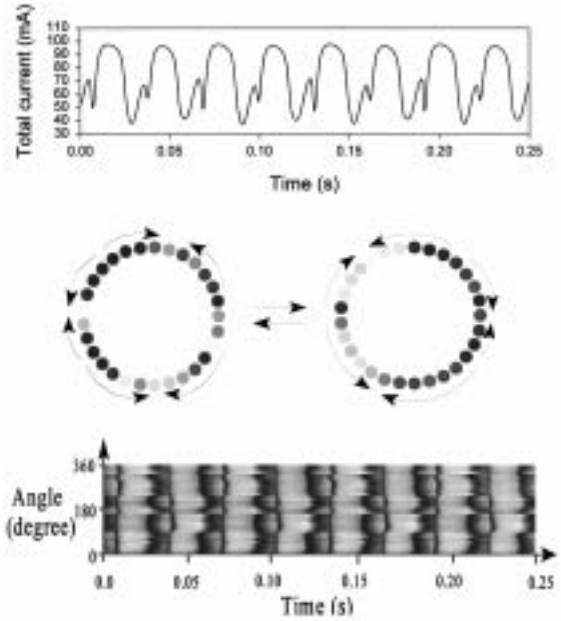

Figure 6. Three-segment wave, $E = -235$ mV (Hg/H_2SO_4), jet speed = 18 cm/s, $[Fe^{2+}] = 0.0$ M. (a) Time series of total current. (b) Snapshot. (c) Current density.

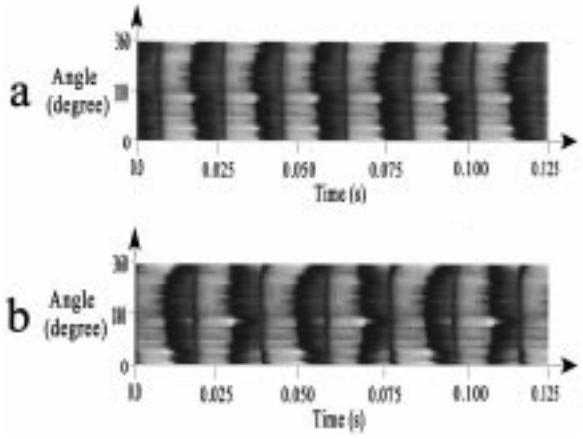

Figure 7. Current space/time dependence. Black represents low current and white high current. (a) Unidirectional wave, $E = -220$ mV. (b) Bidirectional wave, $E = -225$ mV.

total current are periodic. As in the above-described experiments, the currents are not harmonic; the time of high current is again longer than that of low current. A period of overall behavior is approximately 0.05 s and comprises two of the highest maxima in total current (at approximately 115 mA). During a complete cycle, two waves propagate alternately in opposite directions, beginning about at 315° and 45°, respectively, i.e., the current drop alternately begins at these two locations. The spatial phase gradient thus alternates sign in the two half cycles. The behavior is easiest to describe beginning at a high value of the total current corresponding to a light region of the space/time plot. The wave front propagates in one direction, and the total current

drops to its minimum value. The current begins to rise and then goes through a small local minimum; this local minimum can be seen in the time series of total current just after the global minimum and in the spatial patterns of where the thin, uniform dark stripe occurs. The current of all the electrodes then rises approximately uniformly. One-half the cycle is now completed. The second half occurs in the same manner, except that the wave propagates in the opposite direction. Note the alternating convex and concave shape of the leading edge of the broad dark stripes.

Normalized energies, eigenfunctions, and coefficients for the $K-L$ expansion of the data in Figure 4a are shown in Figure 5a. The period is approximately 0.05 s and comprises two of the large minima of the total current time series. (The period also comprises two maxima. However, the low current−dark behavior is easiest to characterize.) The spatiotemporal dynamics can be represented by two terms of the expansion. The first eigenfunction is independent of position and, when multiplied by the time dependent coefficient, could represent the overall time behavior. The second term in the expansion, whose eigenfunction is a function of position, goes through a global minimum preceding every second global minimum of the first coefficient. This phase lead produces the wave propagation in one direction. (Compare, for example, to the coefficients for the wave behavior shown in Figure 3a.) On alternate minima of the first coefficient, the minimum of the second coefficient lags that of the first coefficient and a wave propagates in the opposite direction. A plot of a_1 vs a_2 is shown at the bottom of Figure 5a; the figure is roughly Figure 8 with extra loops in which a_1 goes through two maxima while a_2 goes through one. The progression of the low-current wave, first from one side and then from the other side of the ring, can be seen. Note the two points to the right of this figure where a_1 reaches its maxima at approximately $a_1 = 5.5$. In both cases, the coefficient a_2 has a small value, alternately positive and negative. These states represent a maximum and almost uniform current on the ring. The coefficient a_1 then drops so that the current decreases. On alternate half cycles, the second coefficient a_2 either increases or decreases so that the point where the current decrease occurs is alternately on opposite sides of the ring. The plot is made somewhat more difficult to interpret because of the extra looping motion of the trajectory. The lack of symmetry about the horizontal axis means that the propagations in the two directions across the ring are not identical.

A more complicated periodic behavior occurs as the potential is lowered to −250 mV, as seen in Figure 4b. The total current again goes through two of the highest maxima (here at about 105 mA) during one period. Starting at a maximum in current, two high to low current wave fronts propagate from about 170° and 350° (lower right and upper left) toward each other, meeting at positions 80° and 260°; this is followed by an almost uniform rise in current of all the electrodes. The total current has now gone from one maximum at 105 mA to the next. This is followed by wave fronts starting at 80° and 260° that meet at positions 170° and 350° and the subsequent uniform rise. A complete period has now been finished and the process is repeated.

The decomposition of Figure 4b is shown in Figure 5b. The patterns of Figure 4b have some similarities to those of Figure 4a that were just discussed. In both cases, the current begins to drop alternately at two locations approximately 180° apart during alternate half cycles of the total current; however, the forms of the patterns differ. The decompositions of the two cases can be seen in Figure 5a and 5b. Figure 5b shows a constant first eigenfunction as did Figure 5a. Moreover, the temporal behaviors of the first two coefficients are essentially identical. The only difference is the shape, or position dependence, of the second eigenfunction.

Further lowering of the potential to $E = -300$ mV results in the chaotic behavior shown in Figure 4c. This chaos is different than that seen in Figure 2c. None of the antiphase behavior is seen in Figure 4c; none would be anticipated, however, since the behavior did not arise from a state of antiphase oscillations. Attractors and Fourier transforms made from the total current and from one of the individual electrodes are similar, and thus the local and global chaotic behavior are similar; this is another indication that the long-range coupling has a length scale at least equal to the size of the electrode array. For the decomposition of the chaotic dynamics of Figure 4c (not shown), approximately 15 terms were necessary to reconstruct the behavior.

The types of behavior seen in Figure 4, often preceded by the simple wave pattern seen in Figure 2a, are seen most commonly under the conditions of these experiments. The patterns also occur over large parameter ranges, i.e., over several decades of millivolts, and thus we obtain several examples of each type of behavior in a set of experiments. The sequence of patterns is, however, not completely reproducible. We always see periodic oscillations with one of the spatial patterns shown, and this changes to the chaotic behavior seen in Figure 4c as the potential is lowered. Sometimes, however, one of the states seen in Figures 2a, 4a, and 4b is skipped on the way to chaos. Sometimes other patterns are seen. One such example is shown in Figure 6. We are not sure why the identical sequence is not obtained each time. It is certainly not due to a narrowness of the parameter range over which each type of behavior occurs since these are large as noted above. It is likely due to slight differences in conditions in various experimental runs, although great care is taken to carry out the experiments under identical conditions. The same array was used in all experiments; it was repolished between runs. Nevertheless, the metal is dissolving and thus certain variations are unavoidable. It is possible that multiple oscillatory states occur under the same conditions, although we have no evidence that they do and we have not investigated this possibility in detail.

The state shown in Figure 6 occurred under the same nominal conditions as those of Figure 4. It arose from a simple wave pattern, such as seen in Figure 2a, as the potential was lowered. Further lowering of potential leads to the chaos of Figure 4c. Note in Figure 6 that there are three regions of wave activity. The sizes of these regions are somewhere between (1/3, 1/3, 1/3) and (1/2, 1/4, 1/4); the largest region (starting at 90° in the snapshot on the left) covers approximately 160° and the other two approximately 100° each. Starting at a high value of the total current, there are three wave fronts of high to low current emanating from locations of about 90°, 220°, and 320° which propagate in both directions; this is followed by an almost uniform rise in current on all electrodes. Then, starting at the next current maximum, the same behavior is repeated, but the waves begin approximately at locations where the previous waves ended. The entire behavior can again be seen in Figure 6c; the transitions from dark to light occur almost uniformly, and those from light to dark show three regions, each of which is alternately convex and concave.

Transition between Two Patterns. We will now discuss in somewhat more detail one of the transitions in patterns that occurs, viz., that between the state such as that in Figure 2a in which a single location is always leading in phase (so that the

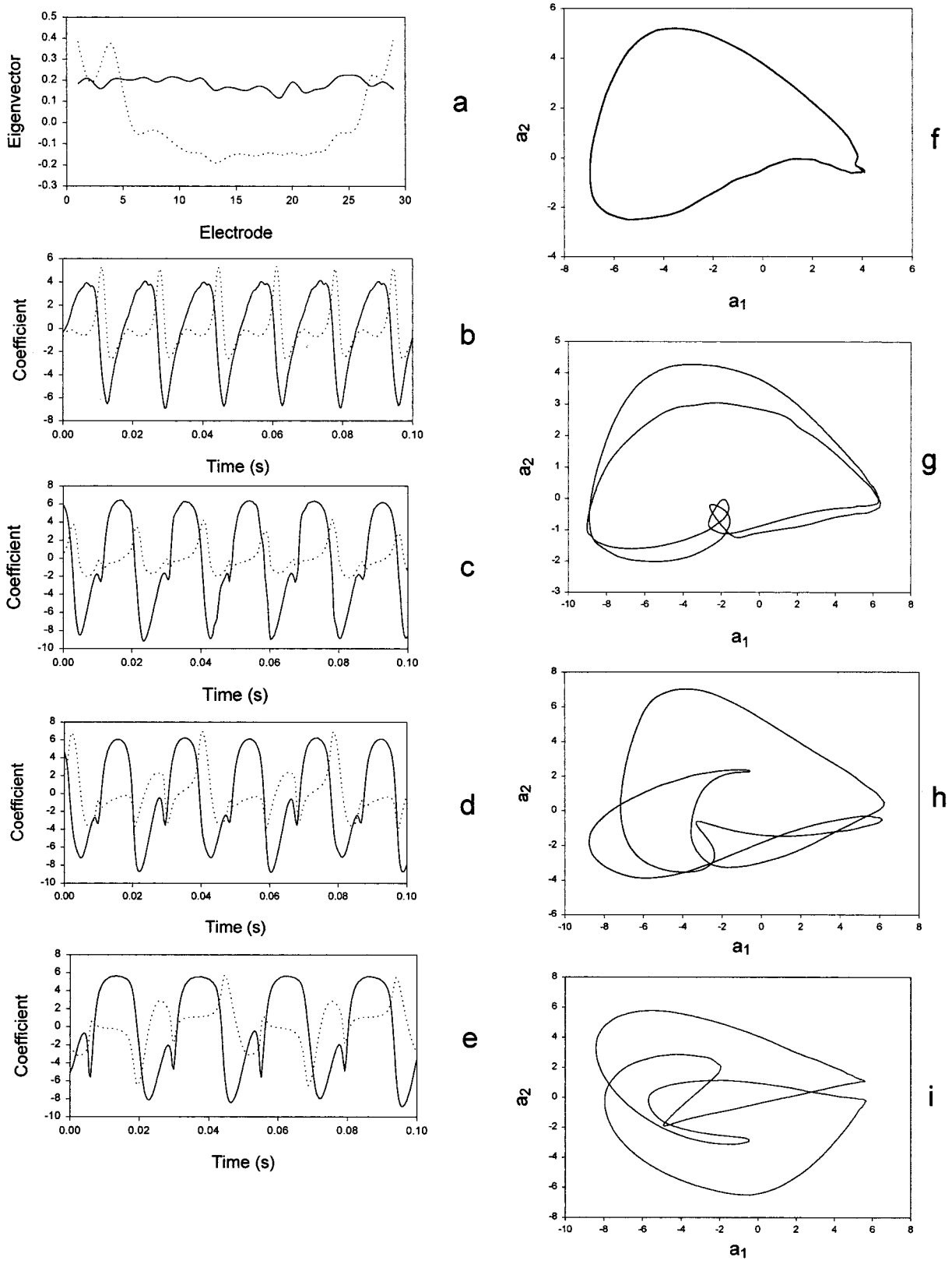

Figure 8. (a) Eigenvectors from pattern in Figure 7a. (b−e) Coefficients from the patterns of Figures 2a, 7a, 7b, and 4a, respectively. Solid line, first term; dotted line, second term. (f−i) Correspond to b−e, respectively.

phase gradient at a point always has the same sign) to the state such as seen in Figure 4a where the point with the phase lead alternates on successive half cycles. The spatial phase gradient in the first case always has the same sign whereas in the second it alternates. This is a transformation from a state in which successive waves at a given location always propagate in the same direction to a state in which alternating waves at the location propagate in opposite directions. To look at the transition more closely, we will consider the results of four experiments carried out at four values of the applied potential at which the behavior of Figures 2a and 4a and two intermediate patterns occur.

The results at the two intermediate conditions are shown in Figure 7 in the form of a space/time plot. These two experiments were done at values of the control parameter differing by 5 mV.

The results for a $K-L$ decomposition are shown in Figure 8. The eigenfunction shown in Figure 8a is that obtained from the data of Figure 7a; however, the eigenfunctions for all four sets of data are essentially equivalent, and so we show only one set. In all cases the dynamics can be described approximately by two terms in the expansion. The first eigenfunction is independent of position (with some experimental variation) in all cases. The second eigenfunction has approximately the same shape in the four cases and can be seen as the dotted line in Figure 8a.

As the potential is changed, the transition is seen in changes in the time-dependent coefficients of the expansion. These are shown in Figure 8 (b−e).

The first coefficient (which multiplies the spatially independent eigenfunction) does change somewhat as we proceed through Figure 8b−e. One change affects the shape of the patterns but apparently does not produce the main feature of the transition. A local minimum appears in the coefficient between the global minimum and global maximum. (Compare Figure 8c to 8b.) This local minimum becomes more pronounced, as seen in Figure 8d and 8e. This mimimum influences the structure of the back of the wave. It causes the thin black stripe that can be seen at the back of each broader black stripe in Figure 4a.

A somewhat more pronounced change occurs in the form of the second time-dependent coefficient as we progress from Figure 8b to 8e. Consider a time at which a_1 is maximal; in all cases a_2 is close to zero, so that the current is large and almost uniform on the ring. As a_1 decreases (the current decreases), the second coefficient in Figure 8b rises so that the one part of the ring first exhibits the decrease in current; every cycle is the same, and the region of decreasing current moves across the ring. In Figure 8c the second coefficient still rises but every other time a_2 has a larger or smaller maximum, respectively. The region of low current still moves every time in the same direction but it is alternately larger and smaller. By Figure 8d, however, the second coefficient is alternately increasing and decreasing as a_1 decreases, although the positive peak is larger than the negative. Every other wave propagates in the opposite direction. In Figure 8e the minimum in a_2 has grown to be approximately as large as the maximum. However, the behavior is still not at this point symmetric and waves in the two-half cycles are not identical.

These changes can be seen in the projections a_1 vs a_2 shown in Figure 8f−i, which correspond to 8b−e, respectively. In Figure 8f, a single simple loop corresponding to the simple wave of Figure 2a is seen. In Figure 8g, an apparent period doubling has occurred; in addition, a small extra loop has arisen, but it is not clear that this has an important effect on the dynamics. In Figure 8h and finally 8i, the transition to the wave motion of Figure 4a is seen.

Discussion

Spatiotemporal patterns, many not previously seen in any type of chemical surface reaction, have been observed on a ring of iron electrodes on which the current could be measured as a function of time and angular position. All the experiments were carried out in the oscillatory region. A uniform oscillatory state in which all elements oscillate synchronously is observed under some conditions, but this state is not the typical behavior. Under most conditions the uniform state is unstable and patterns depending on both time and space arise. (For discussions of such dynamics see, for example, ref 39) The observed periodic behavior can then be represented as a temporal mean, an oscillating uniform component, and higher modes. We observe oscillations in which alternate locations on the ring lead in phase, wave motion on three sections of the ring, and transitions from periodic to chaotic behavior. Antiphase oscillations were also observed. In addition, a sequence of patterns obtained with changes in the applied potential in which a transition including an apparent period doubling was investigated in detail.

The nature of transitions among different spatiotemporal patterns can be made clearer in some cases with the aid of proper orthogonal decomposition. In the transition with change in applied potential from the state in which the local spatial phase gradient had at all times the same sign to one in which the sign alternated on half cycles, it was seen in Figure 8 that the four types of behavior shown all could be represented by the same set of spatially dependent eigenfunctions. The changes between states could then be seen to be due only to changes in the time-dependent coefficients. A period doubling in the time-varying coefficients apparently is the first step in the transitions. In other cases, the transitions are seen more strongly in the spatially varying eigenfunctions; for example, consider the behavior of Figure 4a and 4b which were obtained at two values of the applied potential, all other quantities held constant. Both are period two oscillations. The transition from 4a to 4b occurs with a change in the spatially dependent eigenfunctions with little change in the temporal coefficients.

All the patterns are produced by the combination of (electro)-chemical reaction and coupling among sites. Since the reference electrode is far from the working electrode, three times the diameter of the ring, the long-range coupling directly couples all sites, just as a global coupling would do, although the coupling does depend on distance unlike the global coupling. Note that in the chaotic region the characteristics of the total current, the sum of all the electrodes, is similar to that of each individual electrode. The behavior seen in these experiments is apparently that of a reaction system with strong long-range coupling. It is not yet clear why some of the new patterns seen in this study have not been seen in other systems such as the gas−solid reactions, even those with added global coupling. The dissimilarities might be caused by differences between the types of coupling, possibly by the kinetics of the reactions, or through their combination, or perhaps by some effect not yet explored.

Acknowledgment. This work was supported in part from grants from the National Science Foundation and Chevron Oil Co. We thank Dan Luss and Yannis Kevrekidis for helpful discussions.

References and Notes

(1) Hudson, J. L.; Tsotsis, T. T. *Chem. Eng. Sci.* **1994**, *49*, 1493.
(2) Heathcote, H. L. *J. Soc. Chem. Ind.* **1907**, *26*, 899.
(3) Lillie, R. S. *Science* ***1928***, *67*, 593.
(4) Otterstedt, R. D.; Plath, P. J.; Jaeger, N. I.; Sayer, J. C.; Hudson, J. L. *Chem. Eng. Sci.* **1996**, *51*, 1747.
(5) Flätgen, G.; Krischer, K. *Phys. Rev. E.* **1995**, *51*, 3997.
(6) Lee, H. P.; Nobe, K.; Pearlstein, A. J. *J. Electrochem. Soc.* **1985**, *132*, 1031.
(7) Franck, U. F.; Fitzhugh, R. *Z. Elektrochem.* **1960**, *65*, 156.
(8) Russell, P.; Newman, J. J. *Electrochem. Soc.* **1987**, *134*, 1051.
(9) Wang, Y.; Hudson, J. L. *AIChE J.* **1991**, *37*, 1833.
(10) Koper, M. T. M. *J. Chem. Soc., Faraday Trans.* **1998**, *94*, 1369.
(11) Albahadily, F. N.; Schell, M. *J. Electroanal. Chem.* **1991**, *308*, 151.
(12) Haim, D.; Lev, O.; Pismen, M.; Sheintuch, M. *Chem. Eng. Sci.* **1992**, *47*, 3907.

(13) Hudson, J. L.; Tabora, J.; Krischer, K.; Kevrekidis, I. G. *Phys. Lett. A* **1994**, *179*, 355.
(14) Koper, M. T. M.; Sluyters, J. H. *Electrochim. Acta.* **1993**, *38*, 1535.
(15) Otterstedt, R. D.; Plath, P. J.; Jaeger, N. I.; Hudson, J. L. *Phys. Rev. E* **1996**, *54*, 3744.
(16) Pigeaud, A.; Kirkpatrick, H. B. *Corrosion* **1969**, *25*, 209.
(17) Sayer, J. C.; Hudson, J. L. *Ind. Eng. Chem. Res.* **1995**, *34*, 3246.
(18) Lev, O.; Sheintuch, M.; Pismen, L. M.; Yarnitzky, H. *Nature* **1988**, *336*, 458.
(19) Otterstedt, R. D.; Plath, P. J.; Jaeger, N. I.; Hudson, J. L. *J. Chem. Soc., Faraday Trans.* **1996**, *92*, 2933.
(20) Fei, Z.; Kelly, R. G.; Hudson, J. L. *J. Phys. Chem.* **1996**, *100*, 18986.
(21) Fei, Z.; Hudson, J. L. *J. Phys. Chem B* **1997**, *101*, 10356−10364.
(22) Fei, Z.; Hudson, J. L. *Ind. Chem. Res.* **1998**, *37*, 2172−2179.
(23) Flätgen, G.; Krischer, K. *J. Chem. Phys.* **1995**, *103* (13), 5428.
(24) Mazouz, N.; Krischer, K.; Flätgen, G.; Ertl, G. *J. Phys. Chem. B* **1997**, *101*, 2403.
(25) Mazouz, N.; Flätgen, G.; Krischer, K. *Phys. Rev. E.* **1997**, *55*, 2260.
(26) Otterstedt, R. D.; Plath, P. J.; Jaeger, N. I.; Hudson, J. L. *Lect. Notes Phys.* **1998**, 503.
(27) Otterstedt, R. D.; Green, B. J.; Jaeger, N. I.; Plath, P. J.; Pritzker, M.; Hudson, J. L. *Proceedings of the Symposia on Advances in Mathematical Modeling and Simulation of Electrochemical Processes and Cathodes for Chlorine Processes*; Van Zee, J. W., Fuller, T. F., Foller, P. C.; Hine, F. Eds.; Proceedings Volume Series PV98−10; The Electrochemical Society, Inc., Pennington, NJ, 1998.
(28) Lane, S. L.; Luss, D. *Phys. Rev. Lett.* **1993**, *70*, 830.
(29) Middya, U.; Luss, D.; Sheintuch, M. *J. Chem. Phys.* **1994**, *100*, 3568.
(30) Somani, M.; Liauw, M. A.; Luss, D. *Chem. Eng. Sci.* **1997**, *52*, 2331.
(31) Liauw, M. A.; Somani, M.; Annamalai, J.; Luss, D. *AIChE J.* **1997**, *43*, 1519.
(32) Yamamoto, S. Y.; Surko, C. M.; Maple, M. B.; Pina, R. K. *Phys. Rev. Lett.* **1995**, *74*, 4071.
(33) Sheintuch, M.; Shvartsman, S. *AIChE J.* **1996**, *42*, 1041.
(34) Pratt, W. K. *Digital Image Processing*; John Wiley & Sons: New York, 1985.
(35) Chen, C.-C.; Chang, H.-C. *AIChE J.* **1992**, *38*, 1461.
(36) Chen, C. C.; Wolf, E.; Chang, H.-C. *J. Phys. Chem.* **1993**, *97*, 1055.
(37) Graham, M. D.; Lane, S. L.; Luss, D. *J. Phys. Chem.* **1993**, *97*, 889.
(38) Krischer, K.; Rico-Martinez, R.; Kevrekidis, I. G.; Rotermund, H. H.; Ertl, G. Hudson, J. L. *AIChE J.* **1993**, *39*, 89−98.
(39) Mikhailov, A. S. *Foundations of Synergetics I*, 2nd ed.; Springer: Berlin, 1994; p 89.